

# Robot-assisted ultrasound-guided biopsy on MR-detected breast lesions

M.K. Welleweerd<sup>1</sup>, D.Pantelis<sup>1</sup>, A.G. de Groot<sup>1</sup>, F.J. Siepel<sup>1</sup> and S. Stramigioli<sup>1,2</sup>

**Abstract**—One out of eight women will get breast cancer during their lifetime. A biopsy, a procedure in which a tissue sample is acquired from the lesion, is required to confirm the diagnosis. A biopsy is preferably executed under ultrasound (US) guidance because it is simple, fast, and cheap, gives real-time image feedback and causes little patient discomfort. However, Magnetic Resonance (MR)-detected lesions may be barely or not visible on US and difficult to find due to deformations of the breast. This paper presents a robotic setup and workflow that assists the radiologist in targeting MR-detected breast lesions under US guidance, taking into account deformations and giving the radiologist robotic accuracy. The setup consists of a seven degree-of-freedom robotic serial manipulator equipped with an end-effector carrying a US transducer and a three degree-of-freedom actuated needle guide. During probe positioning, the US probe is positioned on the patient's skin while the system tracks skin contact and tissue deformation. During the intervention phase, the radiologist inserts the needle through the actuated guide. During insertion, the tissue deformation is tracked and the needle path is adjusted accordingly. The workflow is demonstrated on a breast phantom. It is shown that lesions with a radius down to 2.9 mm can be targeted. While MRI is becoming more important in breast cancer detection, the presented robot-assisted approach helps the radiologist to effectively and accurately confirm the diagnosis utilizing the preferred US-guided method.

## I. INTRODUCTION

Breast cancer is one of the most common cancers and the leading cause of cancer death in females [1]. Successful treatment is more likely if the disease is detected and diagnosed in an early stage. While mammography is the most widespread imaging modality for detection, Magnetic Resonance Imaging (MRI) is getting more important. MRI has a higher sensitivity than other imaging modalities and has the potential to overcome the shortcomings of mammography by using new imaging approaches. However, the selectivity of MRI, which is the ability to differentiate between benign and malignant lesions on the acquired images, is not very high. Consequently, a tissue sample from the detected lesion should be acquired to confirm the diagnosis. The preferred procedure to achieve this is the ultrasound (US)-guided biopsy. During this procedure, a biopsy needle is manually inserted by the radiologist and is navigated to the lesion under US guidance. This is the preferred procedure since — compared to an MRI-guided biopsy — it is relatively cheap, simple, fast,

gives real-time feedback and causes little patient discomfort because of the smaller needle diameters used [2].

However, performing a US-guided biopsy on an MR-detected lesion is challenging. Firstly, transferring the lesion position from the MRI to the US image is complicated due to the different patient positioning between imaging modalities; an MRI is typically performed with the patient in prone position, while during a US-guided biopsy the patient is positioned semi-supine. Due to the highly deformable tissue, relating the US images to the MRI is difficult. Furthermore, an MR-detected lesion may be barely visible on the US image [2]. Finally, the procedure is highly operator dependent due to these challenges and therefore finding the lesion may take a significant amount of time.

The field of robotics is progressively becoming more important in healthcare due to its high accuracy, efficiency and operator independency. Specifically, there is an increasing interest in robot-assisted breast biopsies because the US probe can be accurately positioned based on the target location and the needle is accurately manipulated [3]. The biggest challenges in targeting a breast lesion include initial localization of the lesion and deformations of the breast during the procedure.

Firstly, the challenge of initial localization is greatly reduced by performing both the MR-imaging and robotic biopsy with the patient prone position. Not only will involuntary movements such as breathing be less apparent in prone position, it also allows to image the breast in its undeformed state [4]. Additionally, it is easier to relate the breast to the MRI by means of e.g. markers attached to the skin [5].

Secondly, there are two approaches to correct for deformations occurring during the robot-assisted US-guided biopsy procedure: deformation prediction and deformation tracking. Prediction methods are a model-based approach in which the updated position of the lesion based on tissue-probe and tissue-needle interactions is estimated. Subsequently, the planned needle trajectory is optimized for this. Although research on the prediction of deformations resulting from different positioning of the breast or interactions with the breast is ongoing [6], [7], a sufficiently accurate patient-specific prediction model of the interactions of the US probe and the biopsy needle with the breast is currently infeasible. Therefore, robotic solutions depend mainly on deformation tracking. Current robotic breast biopsy systems mostly depend on the visibility of the target [8]–[12] and therefore, any deformations related to probe placement and needle insertion are easily compensated for in these applications; the lesion can be segmented from subsequent US images and the needle trajectory can be adjusted accordingly. Actually, a

<sup>1</sup> is affiliated with the Robotics and Mechatronics group, University of Twente, The Netherlands. Mail: m.k.welleweerd@utwente.nl

<sup>2</sup> is affiliated with the Bio-mechatronics and Energy-Efficient Robotics group, ITMO University, St. Petersburg, The Russian Federation.

This project has received funding from the European Union's Horizon 2020 research and innovation programme under grant agreement No. 688188 (MURAB).

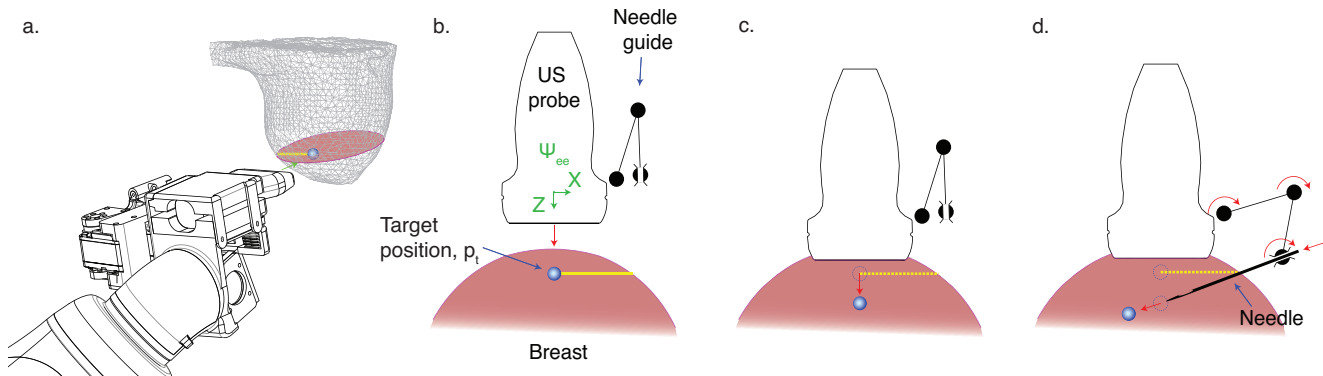


Fig. 1: The approach to a robot-assisted US-guided biopsy on an MR-detected lesion: a. Robotic manipulator approaches breast. In the US plane (b.), the target moves upon positioning the US probe (c.) and inserting the needle (d.).

target can be tracked independently of its visibility by using tissue deformation tracking algorithms. Applicable algorithms that have been implemented in robotic US applications include speckle tracking, optical flow and normalized cross correlation and mutual information similarity functions [13]–[15]. However, those studies do not focus on the whole breast biopsy procedure, i.e. they do not include probe positioning and the resulting deformations.

The purpose of this work is to develop a workflow to accurately perform a robot-assisted US-guided biopsy on MR-detected lesions. The work specifically focuses on how US feedback from the probe can be utilized in the process. US feedback is used in acquiring acoustic coupling, which is the transfer of acoustic energy from the probe into the tissue. Most other studies use a normal force for this. Also, in the absence of accurate deformation prediction models and of the ability to detect the lesion on US images, US feedback is used to compensate for deformations caused by the needle insertion and deformations caused upon probe contact. The lesion is not visible, but its initial position before deformation is retrieved from pre-operative data, such as MRI.

The presented solution utilizes a seven degree-of-freedom (7DOF) serial manipulator equipped with a linear US probe and an actuated needle guide. Confidence maps, previously used for pose adjustments of robotic US systems [16], [17], are utilized to estimate the first probe contact and to correctly place the probe. Upon first probe contact it is assumed that the deformation is not significant. The target, whose position was extracted from pre-operative data, can thus be mapped in the US image and tracked with optical flow during further positioning and needle insertion. The radiologist is responsible for needle insertion, but the actuated needle guide determines the needle trajectory based on kinematics and needle detection. The robot-assisted biopsy workflow is validated with phantom experiments. It is shown that pre-operatively defined targets which are invisible on US images are targeted with millimeter accuracy. The compensation for movements in the 2D US frame is a first step towards compensation for both in- and out-of-plane deformations.

## II. ROBOT-ASSISTED US-GUIDED BIOPSY

The approach for a robot-assisted US-guided biopsy on an MR-detected lesion is shown in Fig. 1. A patient is positioned in prone position over a robotic serial manipulator carrying an end-effector (EE) equipped with a US probe and a 3DOF actuated needle guide [18]. The guide aims the needle towards a target within the US plane. The lesion’s position with respect to the robot is known by registration of the MRI-data with the patient by e.g. a camera scan. A desired US plane through the lesion is defined and a contact point of the US probe with the skin is derived such that the target is in the field of view (FOV) (Fig. 1 a.). The robot is aligned with the desired US plane (Fig. 1 b.) and approaches the breast. It is shown that during probe positioning (Fig. 1 c.) and needle insertion (Fig. 1 d.) the target displaces with respect to its original estimated position. These two phases of the biopsy, and how to compensate for the target displacement, will be discussed in the following sections.

### A. Probe positioning

The probe positioning phase is focused on aligning the EE with the desired US plane, measuring the instant of contact and starting to track tissue deformations. Additionally, it assures adequate acoustic coupling between the US probe and the skin in its final position. The probe’s position and orientation remain static during needle insertion.

1) *Determining the contact position:* A triangular mesh, which describes the skin surface of the breast, and the target position,  $p_t$ , are extracted from the pre-operative data (Fig. 1 a. and b.). The desired US-plane,  $A$ , is constrained by the target position such that  $p_t \in A$ . The orientation of  $A$  is based on input of the radiologist, who could e.g. prefer  $A$  to be aligned with the coronal plane. Possible contact positions are extracted by calculating the intersection of  $A$  with the surface model. The initial contact position is also chosen by the radiologist. The robotic manipulator aligns the x- and z-axis of the EE frame,  $\Psi_{ee}$  in Fig. 1, with  $A$ . It is assumed that if the contact point of the probe with the skin and the target location are coincident with the z-axis of  $\Psi_{ee}$ , the lesion will be in the FOV upon contact. Thus, at the moment of contact, the target coordinates can be associated with a pixel in the US image.

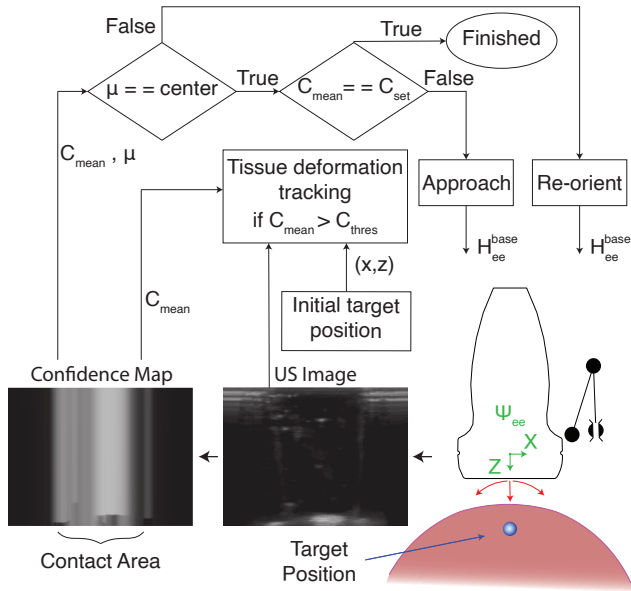


Fig. 2: System diagram of the probe positioning phase. The features of the confidence map are used to adjust the probe position and to start deformation tracking. The US image is used to track the tissue deformation. The process stops if full contact is achieved.

2) *Acquiring contact*: The system diagram for acquiring contact is shown in Fig. 2. Confidence maps are utilized to estimate the moment of contact and to gain acoustic coupling with the breast. The confidence map,  $C$ , represents the per pixel confidence in the corresponding US image,  $U$ . The pixels of an image are located in a matrix  $\Omega^{n \times m}$ . An acquired US image,  $U : \Omega \rightarrow [0, 1]$ , is associated with a confidence map,  $C : \Omega \rightarrow [0, 1]$ . The map,  $f : U \rightarrow C$ , is solved as a random walk equilibrium which respects physical constraints specific to US. Furthermore, the top row of a confidence map is defined as 1 and the bottom row is defined as 0 [19]. Confidence maps emphasize shadowed and attenuated regions, and are therefore useful to estimate how the probe is in contact with the skin. As shown in Fig. 2, partial contact transfers to a high confidence region in the middle of the confidence map. The mean confidence,  $C_{\text{mean}}$ , correlates with the contact area of the US probe with the skin

$$C_{\text{mean}} = \frac{1}{n \cdot m} \sum_{(i,j) \in \Omega} C(i, j). \quad (1)$$

During the positioning of the probe,  $C_{\text{mean}}$  is constantly evaluated. Fig. 2 shows that a threshold value of the mean confidence,  $C_{\text{thres}}$ , is defined which indicates the first contact and the start of tissue deformation tracking. Additionally,  $C_{\text{set}}$  is defined as the mean confidence for which the probe has appropriate acoustic coupling with the breast.

Furthermore, the weighted barycentre,  $\mu$ , of the confidence indicates where the contact with the probe is located

$$\begin{aligned} \mu_i &= \frac{1}{C_{\Omega}} \sum_{(i,j) \in \Omega} i \cdot C(i, j), \\ \mu_j &= \frac{1}{C_{\Omega}} \sum_{(i,j) \in \Omega} j \cdot C(i, j), \end{aligned} \quad (2)$$

with  $C_{\Omega} = \sum_{(i,j) \in \Omega} C(i, j)$  the total confidence. The pixel indices  $\mu_i$  and  $\mu_j$  correspond to EE coordinates  $\mu_z$  and  $\mu_x$ , respectively. If these coordinates are located off-centre, the probe contact is off-centre and thus the target may not be in the FOV. Therefore, the probe should be rotated around the target by  $\theta_r = \tan^{-1} \frac{\mu_x}{\mu_z}$  radians. This movement is indicated in Fig. 2. The new desired position relative to the current position expressed in  $\Psi_{\text{ee}}$  is given by

$$H_d^c = \begin{bmatrix} I^{3 \times 3} & -d_t \hat{z} \\ 0^{1 \times 3} & 1 \end{bmatrix} \begin{bmatrix} Rot_y(\theta_r)^{3 \times 3} & 0^{3 \times 1} \\ 0^{1 \times 3} & 1 \end{bmatrix} \begin{bmatrix} I^{3 \times 3} & d_t \hat{z} \\ 0^{1 \times 3} & 1 \end{bmatrix}, \quad (3)$$

where  $I$  is the identity matrix,  $\hat{z}$  the unit vector in z-direction and  $d_t$  is the distance between the EE and the target. Once the barycentre is located in the centre, the robot approaches the breast until the mean confidence matches  $C_{\text{set}}$ .

3) *Tissue deformation tracking*: It is assumed that no significant deformation has taken place when  $C_{\text{mean}} = C_{\text{thres}}$ . Thus, the target,  $p_t$ , still has its pre-operatively defined position. Therefore, the target coordinates  $(z, x)$  expressed in  $\Psi_{\text{ee}}$ , as obtained from the pre-operative data, can be mapped on a pixel  $(i, j)$  of the US image  $U$ . The probe continues to move to acquire acoustic coupling. This motion compresses the tissue and thus moves the target from its original position. Since the target may not be visible, optical flow is used to track this motion. The popular Lucas-Kanade method is used [20] to track the movement of brightness patterns of the target location. This method assumes that the inter-frame movements are small and the same for a small window of pixels with the target at its centre. A pyramidal implementation of the algorithm is utilized to make the target tracking more robust [21]. The algorithm outputs an updated position of the expected target location per acquired US image. The same tissue tracking algorithm is also utilized during needle insertion.

## B. Needle insertion

After probe positioning, the radiologist starts inserting the needle. The system diagram is shown in Fig. 3. The initial target position is the position of the target determined after probe positioning. The needle may displace the target due to tissue-needle interaction and thus the US images are evaluated to update the target position. Furthermore, the actual needle trajectory may differ from the one derived with the forward kinematics due to needle bending. Therefore, the system relies on a needle detection algorithm also.

1) *Needle trajectory*: As shown in Fig. 3, the desired needle trajectory, expressed in the needle guide frame  $\Psi_{\text{ng}}$ , is defined by the insertion point  $p_i = (x_i, y_i)$  and the target position  $p_t = (x_t, y_t)$  as

$$y - y_t = \frac{y_i - y_t}{x_i - x_t} (x - x_t). \quad (4)$$

The insertion position is located on the intersection of plane  $A$  with the surface model of the breast, and is chosen by the radiologist. Throughout needle insertion, this position is kept constant, while the target position is updated according to

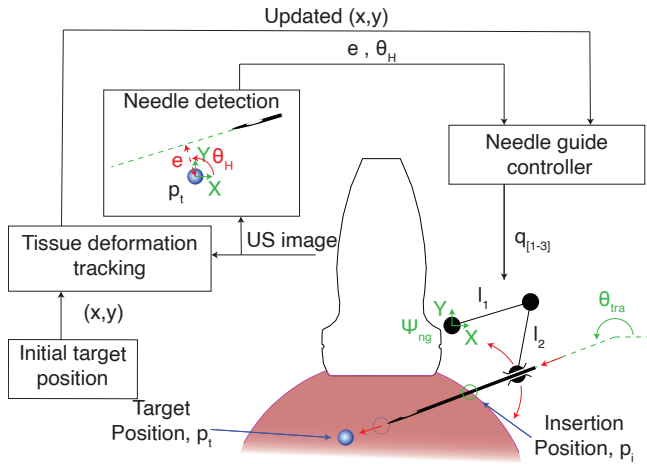


Fig. 3: System diagram of the needle insertion phase. The controller adjusts the needle guide based on optical flow and needle detection. The insertion position remains constant, such that no stress is exerted on the skin.

the tissue motions. This way, the centre of motion is a point on the skin, and thus the needle will not cause any stress in this position. This resembles the way a radiologist would manually manipulate the needle.

2) *Needle detection*: The needle detection is broken down in several steps. First, Canny edge detection is applied to the US image [22]. Canny edge detection consists of the following processing steps: the application of a Gaussian filter to reduce the noise, finding the intensity gradients of the image along the  $x$ - and  $y$ -axis, finding the sharpest edges, applying a double threshold to remove edge pixels caused by noise and finishing the edges by connecting the stronger edges with weaker ones. In the resulting image, the needle trajectory is found by the Hough transform, and the error between the needle trajectory and the target is expressed as

$$e = x \cos \theta_H + y \sin \theta_H, \quad (5)$$

with  $e$  the shortest distance between the target and the trajectory and  $\theta_H$  the angle between the  $x$ -axis and the normal connecting the target and the trajectory, as presented in see Fig. 3 [23]. The target,  $p_t$ , is taken as the origin.

A controller adjusts the needle trajectory virtually moving the target position,  $p_t$ , in the direction opposite to the normal defined by  $e$  and  $\theta_H$ . The offset to the needle trajectory remains constant if no needle is detected in the image.

3) *Needle guide position*: The needle guide's position,  $p_{ng}$ , is located at a constant distance,  $d_{ng}$ , of the insertion point,  $p_i$ , such that

$$p_{ng} = \begin{bmatrix} x_{ng} \\ y_{ng} \end{bmatrix} = p_i - \begin{bmatrix} d_{ng} \sin \theta_{tra} \\ d_{ng} \cos \theta_{tra} \end{bmatrix}, \quad (6)$$

where  $\theta_{tra}$  is the angle of the needle trajectory with the  $x$ -axis of  $\Psi_{ng}$  as shown in Fig. 3. The guide's joint positions are

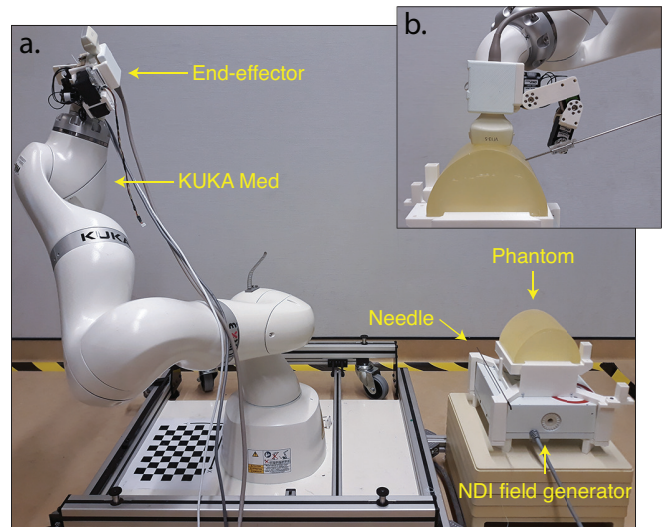


Fig. 4: The robotic setup. a. Overview of the setup with indicated: the KUKA LBR Med 7 with the end-effector attached, the NDI field generator, the tracked needle and the breast phantom. b. Close up of the EE with the needle inserted in the phantom.

acquired via the inverse kinematics of the 2D planar system

$$\begin{aligned} q_1 &= \arctan 2(y, x) \pm \beta, & \beta &= \cos^{-1} \left( \frac{r^2 + l_1^2 - l_2^2}{2l_1 r} \right), \\ q_2 &= \pi \pm \alpha, & \alpha &= \cos^{-1} \left( \frac{l_1^2 + l_2^2 - l_2^2}{2l_1 l_2} \right), \\ q_3 &= \theta_{tra} - q_1 - q_2, \end{aligned} \quad (7)$$

in which  $r = \sqrt{x_{ng}^2 + y_{ng}^2}$ ,  $l_1$  and  $l_2$  are the lengths of link 1 and 2, respectively,  $q_i$  indicates the joint position of the  $i$ -th joint, and the signs for  $\alpha$  and  $\beta$  should agree [24].

### III. EXPERIMENTAL VALIDATION

#### A. Experimental setup

The setup (Fig. 4) consists of a 7DOF robotic manipulator (KUKA Med 7 R800, KUKA GmbH, Germany) to which the EE is connected. The EE holds a VF13-5 linear US probe (Siemens AG, Germany) and is equipped with a 3DOF needle guide. The transformation of both the transducer and the needle guide with respect to the flange is retrieved from the CAD design of the EE. The US probe is connected to an X300 US system (Siemens AG, Germany) which streams the US images with an update rate of 24 Hz to a workstation via a capture card (Pro Capture DVI HD, Magewell, China). The workstation communicates with the manipulator via the fast research interface, and with the EE via serial communication.

A phantom with a simplified breast shape, such that the deformations occurring during the procedure remain in-plane, is constructed with a PVC/Plasticizer mixture (Bricoleurre, France). The breast's skin is mimicked by a stiff outer layer of approximately 10 mm (100% / 0%), and the adipose tissue by a softer inner structure (70% / 30%). While the skin layer is expected to have a comparable stiffness to actual skin, the inner structure may be up to ten times stiffer than actual

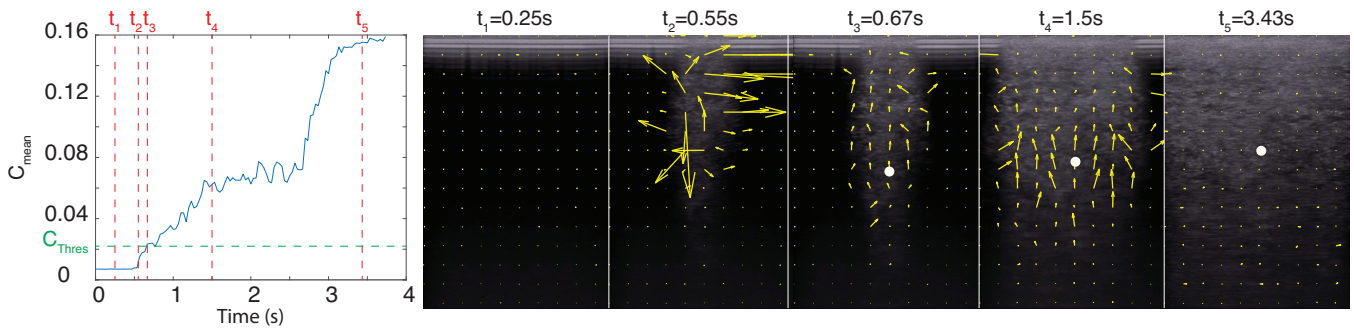


Fig. 5: Graph showing the average confidence while approaching the breast and the corresponding US images for  $t_{[1-5]}$ . The yellow arrows indicate the optical flow profile. The white dot is the tracked target starting from  $C_{\text{mean}} = C_{\text{thres}}$ .

adipose tissue [25]–[27]. 1 wt.% silica powder is added to both mixtures to increase scattering.

The phantom was placed on top of and registered with an Aurora tracker (Northern Digital Inc., Canada). An electromagnetic (EM) tracker (part nr: 610090, Northern Digital Inc., Canada) was placed inside the phantom at a depth of approximately 25 mm to function as a lesion with zero volume and a known location. The robot is registered with the Aurora tracker such that the initial lesion location with respect to the robot is known. A custom biopsy needle was produced utilizing a metal tube with an outer diameter of 2 mm and equipped with an EM tracker (part nr: 610059). The experiments were performed in supine position since the bed interferes with the NDI equipment, but normally the procedure is performed in prone position. The desired contact position was based on the current target position and the CAD-file of the phantom. In all needle insertion experiments, the accuracy of the procedure is determined by recording the positions of both sensors and determining the Euclidean distance between the needle tip and the target. Furthermore, the normal distance is determined, which is the shortest distance between the target and the needle trajectory.

### B. Experiments

Three experiments were conducted. The first experiment determines the accuracy of the estimated target location with respect to the actual target location after probe positioning. Starting from its home position, the robot aligns the EE with the indicated US-plane and brings the probe in contact with the phantom. The second experiment determines the in-plane accuracy of the needle placement. This experiment has been performed with and without the needle detection activated. The needle is unlikely to bend during this particular experiment due to the soft phantom and stiff needle. Therefore, a small uniformly distributed error of  $\pm 0.08$ ,  $\pm 0.06$  and  $\pm 0.03$  rad has been added to the initial setpoints of joint one, two and three, respectively. The third experiment determines the accuracy of the whole workflow. Each experiment has been performed ten times and averaging is applied.

### C. Results

Fig. 5 presents the mean confidence during an approach to the phantom accompanied with US images and their

corresponding optical flow profiles at times  $t_{[1-5]}$ . At  $t_1$  and  $t_2$ , it is shown that the optical flow profile does not follow the deformation. However, at  $t_3$ , when  $C_{\text{mean}} = C_{\text{thres}}$ , and  $t_4$  the profile in the centre of the image matches the deformation and the target, shown in white, moves along. In TABLE I, the error between the tracked target position and the actual target position is stated for the initial position, when  $C_{\text{mean}} = C_{\text{thres}}$  and the final position, when  $C_{\text{mean}} = C_{\text{set}}$ . It shows that the initial error is in the millimeter range, indicating that the target to robot registration has millimeter accuracy. Furthermore it seems that, based on this data, a larger target displacement does not necessarily imply a larger error. The target displacement is the largest in z-direction, whereas the error in z-direction is not. Actually, the x-direction has the largest error, because the tracked position sometimes follows the expanding region, indicated by the horizontal arrows of the optical flow profiles shown in Fig. 5 at  $t_3$  and  $t_4$ .

TABLE II shows that the needle placement is more accurate without needle detection than with. This is due to the detection

TABLE I: Mean absolute error between the estimated lesion position and the actual lesion position initially, when  $C_{\text{mean}} = C_{\text{thres}}$ , and finally, when  $C_{\text{mean}} = C_{\text{set}}$ , and the target displacement during the procedure.

		$d_x$ [mm]	$d_y$ [mm]	$d_z$ [mm]
		mean (max)	mean (max)	mean (max)
Error	Initial	1.03 (1.28)	0.59 (1.82)	1.23 (1.71)
	Final	2.12 (3.69)	0.80 (1.98)	0.97 (3.05)
Target displacement		0.53 (2.47)	0.88 (2.99)	2.35 (8.61)

TABLE II: Mean absolute distance between the needle tip and NDI target after needle insertion

Needle detection	$d_x$ [mm]	$d_z$ [mm]	$d_{\text{norm}}$ [mm]
	mean (max)	mean (max)	mean (max)
✗	0.72 (1.44)	0.76 (2.05)	0.76 (2.15)
✓	1.81 (3.12)	1.61 (4.60)	1.54 (3.14)

TABLE III: The mean absolute distance of the needle tip, and the normal distance of the needle trajectory with respect to NDI target, after completing the procedure in which the probe is placed and the needle is inserted. Additionally, the target displacement is noted.

	$d_x$ [mm]	$d_y$ [mm]	$d_z$ [mm]	$d_{\text{norm}}$ [mm]
	mean (max)	mean (max)	mean (max)	mean (max)
Total error	1.15 (2.84)	1.31 (3.53)	3.47 (5.05)	2.89 (4.88)
Target displ.	0.84 (2.52)	0.93 (3.32)	2.66 (9.13)	

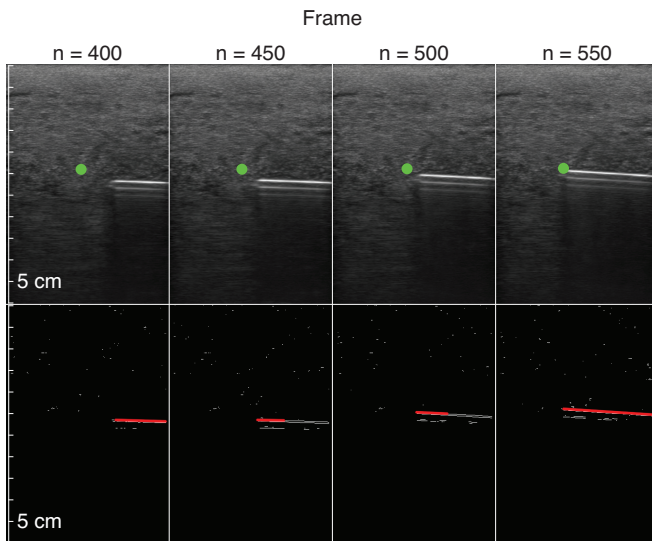


Fig. 6: Image sequence showing the needle trajectory adjustment based on needle detection. Both the US image with the tracked point and the processed image with the detected needle are shown. The frame rate was 20 Hz.

algorithm marking the top edge — not the core — of the needle, which is then aligned with the target (Fig. 6). Hence, the core of the needle is off by the needle radius.

TABLE III presents the accuracy of the entire workflow, in which the robotic manipulator first positions the US probe to view the target, and then guides the needle towards the target. At this moment, the error is not directly related to the errors found in TABLE I and II. Additional experiments may find this relation.

#### IV. DISCUSSION

This study demonstrated an approach to a robot-assisted US-guided biopsy on MR-detected lesions which may be hard to target otherwise. The overall accuracy, as presented in Table III, indicates that it is feasible to target lesions with a radius down to 3 mm. This accuracy is acceptable in breast cancer diagnostics and similar to equivalent experiments performed in the cited studies (1.1–2 mm) [8], [9]. The accuracy could be increased by improving the registration between the phantom and the robot, which is currently in the millimeter range. Other factors influencing the accuracy are the target tracking, the calibration of the US probe and the needle guide with the robot flange, and the accuracy of the needle guide itself.

The main limitation of this study is the assumption that the lesion remains in-plane. This assumption was correct for the performed experiments since the phantom and the applied forces were symmetric. However, in real-life situations the tumor may move out-of-plane due to asymmetry in the applied pressure and the boundary conditions. Nonetheless, the system can easily be extended to 3D by switching to a 3D US probe. Both confidence maps and deformation tracking have previously been applied to 3D US. Additionally, out-of-plane motions may be detected from the B-mode images by taking the divergence of the optical flow field. In future steps, both simulation and feedback algorithms may be combined to account for deformations that the current system cannot.

Furthermore, the deformation in breast tissue is larger than in phantom material: the structure is less constrained, the material softer, and although positioned in prone position, the patient may move. Therefore, the manipulator may need to adjust the probe position and subsequently the needle guide during needle insertion to retain acoustic coupling. Impedance control of the needle guide may provide compliance for small patient movements, but will affect the accuracy. Also, a safety release mechanism may be needed for the needle in a clinical environment, since the patient may inadvertently move more than the system accounts for.

This work specifically focused on how US feedback can be integrated to estimate probe contact and compensate for deformations. It showed that confidence maps are suitable to both estimate probe contact and acquire acoustic coupling with the phantom. The confidence map has advantages over force feedback, since variations in breast stiffness will not influence the image quality while deformations are kept to a minimum. Fig. 5 shows how the confidence map serves to start the tissue tracking. The optical flow profile shows the tissue compression in the region in contact, whereas the edges show some vectors pointing sideways indicating the expanding region in contact. Sometimes, the tracked target moved along horizontally with this region. This can be prevented by specifically evaluating the confidence around the target area, by setting  $C_{\text{thres}}$  to a higher value and by having a more accurate registration between the target and the robot. Optical flow was also successfully applied during needle insertion. TABLE II shows that in-plane accuracy of the needle placement is currently more accurate with than without needle detection. This is because the implemented algorithm detects and aligns the top edge of the needle with the target, whereas the forward kinematics considers the centre of the needle. The needle detection will be more accurate by incorporating the needle radius in the error,  $e$ , in equation 5.

Overall, the system shows some promising features. The robot-assisted biopsy minimizes the MR-time, since the biopsy takes place under US guidance, the time per biopsy is less, because the system automatically navigates to the correct US plane, and the radiologist gains robotic accuracy, even while he is in control like in the conventional procedure. Thus, the radiologist can still respond appropriately to either haptic or patient feedback.

#### V. CONCLUSION

A robotic workflow was introduced to assist the radiologist to accurately perform an US guided biopsies on MR-detected lesions. It was shown confidence maps can be utilized to estimate first probe contact, and that optical flow can track tissue deformation in areas with high confidence with millimeter accuracy. The needle detection algorithm did reduce errors in the initial direction of the needle, but at this point is less accurate than using only the encoders of the needle guide. The proposed workflow has millimeter accuracy in the current setting.

## REFERENCES

- [1] F. Bray, J. Ferlay, I. Soerjomataram, R. L. Siegel, L. A. Torre, and A. Jemal, "Global cancer statistics 2018: GLOBOCAN estimates of incidence and mortality worldwide for 36 cancers in 185 countries," *CA: A Cancer Journal for Clinicians*, vol. 68, no. 6, pp. 394–424, nov 2018.
- [2] V. Y. Park, M. J. Kim, E.-K. Kim, and H. J. Moon, "Second-Look US: How to Find Breast Lesions with a Suspicious MR Imaging Appearance," *RadioGraphics*, vol. 33, no. 5, pp. 1361–1375, sep 2013.
- [3] M. Z. Mahmoud, M. Aslam, M. Alsaadi, M. A. Fagiri, and B. Alonazi, "Evolution of Robot-assisted ultrasound-guided breast biopsy systems," *Journal of Radiation Research and Applied Sciences*, vol. 11, no. 1, pp. 89–97, jan 2018.
- [4] T. R. Nelson, A. Tran, H. Fakourfar, and J. Nebeker, "Positional Calibration of an Ultrasound Image-Guided Robotic Breast Biopsy System," *Journal of Ultrasound in Medicine*, vol. 31, no. 3, pp. 351–359, mar 2012.
- [5] T. E. Chemaly, F. J. Siepel, S. Rihana, V. Groenhuis, F. van der Heijden, and S. Stramigioli, "MRI and stereo vision surface reconstruction and fusion," in *2017 Fourth International Conference on Advances in Biomedical Engineering (ICABME)*. IEEE, oct 2017, pp. 1–4.
- [6] B. Eiben, V. Vavourakis, J. H. Hipwell, S. Kabus, C. Lorenz, T. Buelow, and D. J. Hawkes, "Breast deformation modelling: comparison of methods to obtain a patient specific unloaded configuration," in *Medical Imaging 2014: Image-Guided Procedures, Robotic Interventions, and Modeling*, Z. R. Yaniv and D. R. Holmes, Eds., vol. 9036, no. March 2014, mar 2014, p. 903615.
- [7] E. Tagliabue, D. Dall'Alba, E. Magnabosco, C. Tenga, I. Peterlik, and P. Fiorini, "Position-based modeling of lesion displacement in ultrasound-guided breast biopsy," *International Journal of Computer Assisted Radiology and Surgery*, vol. 14, no. 8, pp. 1329–1339, 2019.
- [8] G. Megali, O. Tonet, C. Stefanini, M. Boccadoro, V. Pappaspyropoulos, L. Angelini, and P. Dario, "A Computer-Assisted Robotic Ultrasound-Guided Biopsy System for Video-Assisted Surgery," in *Lecture Notes in Computer Science (including subseries Lecture Notes in Artificial Intelligence and Lecture Notes in Bioinformatics)*. Springer, 2001, vol. 2208, pp. 343–350.
- [9] J. Kettenbach, G. Kronreif, M. Figl, M. Fürst, W. Birkfellner, R. Hanel, and H. Bergmann, "Robot-assisted biopsy using ultrasound guidance: initial results from in vitro tests," *European Radiology*, vol. 15, no. 4, pp. 765–771, apr 2005.
- [10] M. Abayazid, P. Moreira, N. Shahriari, S. Patil, R. Alterovitz, and S. Misra, "Ultrasound-guided three-dimensional needle steering in biological tissue with curved surfaces," *Medical Engineering & Physics*, vol. 37, no. 1, pp. 145–150, jan 2015.
- [11] V. Mallapragada, N. Sarkar, and T. Podder, "Robot-Assisted Real-Time Tumor Manipulation for Breast Biopsy," *IEEE Transactions on Robotics*, vol. 25, no. 2, pp. 316–324, apr 2009.
- [12] K. Liang, A. J. Rogers, E. D. Light, D. von Allmen, and S. W. Smith, "Three-Dimensional Ultrasound Guidance of Autonomous Robotic Breast Biopsy: Feasibility Study," *Ultrasound in Medicine & Biology*, vol. 36, no. 1, pp. 173–177, jan 2010.
- [13] A. Krupa, G. Fichtinger, and G. D. Hager, "Real-time Motion Stabilization with B-mode Ultrasound Using Image Speckle Information and Visual Servoing," *The International Journal of Robotics Research*, vol. 28, no. 10, pp. 1334–1354, oct 2009.
- [14] Z. Neubach and M. Shoham, "Ultrasound-Guided Robot for Flexible Needle Steering," *IEEE Transactions on Biomedical Engineering*, vol. 57, no. 4, pp. 799–805, apr 2010.
- [15] M. Kaya, E. Senel, A. Ahmad, and O. Bebek, "Visual tracking of multiple moving targets in 2D ultrasound guided robotic percutaneous interventions," in *2017 IEEE International Conference on Robotics and Automation (ICRA)*. IEEE, may 2017, pp. 1996–2002.
- [16] P. Chatelain, A. Krupa, and N. Navab, "Confidence-Driven Control of an Ultrasound Probe," *IEEE Transactions on Robotics*, vol. 33, no. 6, pp. 1410–1424, dec 2017.
- [17] S. Virga, R. Göbl, M. Baust, N. Navab, and C. Hennemperger, "Use the force: deformation correction in robotic 3D ultrasound," *International Journal of Computer Assisted Radiology and Surgery*, vol. 13, no. 5, pp. 619–627, may 2018.
- [18] M. K. Welleweerd, F. J. Siepel, V. Groenhuis, J. Veltman, and S. Stramigioli, "Design of an end-effector for robot-assisted ultrasound-guided breast biopsies," *International Journal of Computer Assisted Radiology and Surgery*, feb 2020.
- [19] A. Karamalis, W. Wein, T. Klein, and N. Navab, "Ultrasound confidence maps using random walks," *Medical Image Analysis*, vol. 16, no. 6, pp. 1101–1112, aug 2012.
- [20] B. D. Lucas and T. Kanade, "Iterative Image Registration Technique With an Application To Stereo Vision." in *IJCAI*, vol. 2, no. September, 1981, pp. 674–679.
- [21] J.-Y. Bouget, "Pyramidal implementation of the affine Lucas Kanade feature tracker," *Intel*, 2000.
- [22] J. Canny, "A Computational Approach to Edge Detection," *IEEE Transactions on Pattern Analysis and Machine Intelligence*, vol. PAMI-8, no. 6, pp. 679–698, nov 1986.
- [23] R. O. Duda and P. E. Hart, "Use of the Hough transformation to detect lines and curves in pictures," *Communications of the ACM*, vol. 15, no. 1, pp. 11–15, jan 1972.
- [24] R. M. Murray, Z. Li, and S. S. Sastry, *A Mathematical Introduction to Robotic Manipulation*. CRC Press, dec 1994.
- [25] A. Gefen and B. Dilmoney, "Mechanics of the normal woman's breast," *Technology and Health Care*, vol. 15, no. 4, pp. 259–271, jul 2007.
- [26] A. Samani, J. Zubovits, and D. Plewes, "Elastic moduli of normal and pathological human breast tissues: An inversion-technique-based investigation of 169 samples," *Physics in Medicine and Biology*, vol. 52, no. 6, pp. 1565–1576, 2007.
- [27] W. Li, B. Belmont, and A. Shih, "Design and Manufacture of Polyvinyl Chloride (PVC) Tissue Mimicking Material for Needle Insertion," *Procedia Manufacturing*, vol. 1, pp. 866–878, 2015.